Study the Enhancement on Corrosion Protection by Adding PFDTES to Hybrid Sol-Gel on AA2024-T3 Alloy in 3.5% NaCl Solutions

Magdi H. Mussa [1], Yaqub Rahaq [2], Sarra Takita [3], Nicholas Farmilo [4]
Materials and Engineering Research Institute, Sheffield Hallam University, Howard Street, Sheffield S1 1WB, U.K.[1]
Mechanical Engineering Department, Sok Alkhamis Imsehel High Tec. Institute, Tripoli, Libya[2, 3, 4]
* Corresponding Author: magdimosa1976@gmail.com

***Abstract*— Sol-gel as protective coatings has been shown to exhibit excellent chemical stability combined with the ability to reduce the corrosion of metal substrates. The sol-gel method is an eco-friendly technique route for producing surface coatings, showing high potential for the replacement of toxic pre-treatment coatings. This study aims to develop a new understanding of the enhancement in corrosion protection of a hybrid-organic-inorganic sol-gel coating that cured at (80oC) by increasing the hydrophobicity and characterized the performance on the aluminium 2024-T3 alloy. The alternative method involved a novel sol-gel was prepared by introducing a 1H,1H,2H,2Hperfluorodecyltriethoxy silane (PFDTES) into the base hybrid sol-gel created from tetraethylorthosilicate silane (TEOS) and triethoxymethyl silane (MTMS) precursors. The results of electrochemical testing analyses reveal the new open finite-length diffusion circuit element (O) coming from electrolyte media diffusion preventive by fluorinated groups. Also, it is revealed increases in corrosion protection arising from the increasing the hydrophobicity of the fluorinated sol-gel coating when it compared to other formula cured under similar conditions. Additionally, the modified sol-gel exhibited improved resistance to cracking, while the increased hydrophobicity may also promote self-cleaning.**

Keywords —Sol-gel, corrosion protection, hydrophobicity, time-constant, finite-length diffusion circuit, electrochemical testing.

I. INTRODUCTION

Assets such as offshore platforms, pipelines and operating facilities are subject to recurrent and severe corrosion attack and biofouling. The previously established method for corrosion protection, which utilized hexavalent chromium-based corrosion inhibitors, is now banned entirely in these industries. Moreover, considerable efforts have been made to replace conventional conversion coatings (i.e., phosphating and chromating) for the corrosion protection of metallic surfaces. Electrochemical analysis methods have been extensively used to facilitate the development of new and novel corrosion preventive coatings based on, for instance, polyaniline, polythiophene, and polypyrrole as corrosion inhibitors [1].

In the last decade, the phenomenon of hydrophobicity has been used to impart corrosion protection, and further studies have investigated the effect of super-hydrophobicity by anodizing the surface of aluminium alloys. Other investigations have studied the surface modification of magnesium alloys via a simple one-step hydrothermal method using an eco - friendly agent, and by using SiO2 nanoparticles incorporated into a hybrid polymeric m matrix fabricated using acrylic resin [2]-[4].

A further driver for the interest in hydrophobic surfaces and coatings has existed since the end of the 1990s when the International Maritime Organization (IMO) adopted a resolution from the Marine Environment Protection Committee (MEPC) [5]. Hydrophobicity has a key role to play in reducing the level of interfacial adhesion between the biocorrosion organisms and submerged surfaces, permitting their ease removal during relative motion between the coated artefact and water, or washing with pressurized water jets [6]. Sol-gel derived coatings have already been identified as a potential solution for the marine industry, where both anti-fouling and corrosion resistance, combined with low environmental impact, is required [7]–[9].

Sol-gel protective coatings on metallic surfaces can improve the corrosion resistance of the Substrate in various corrosive media. The sol-gel process is an eco-friendly method of surface protection, which offers various possibilities, including single-layer coating systems with anti-corrosion or anti-fouling properties, or bilayer coating systems with dual-protection and multi-function coating systems for marine and aerospace use [8], [10]–[12]. Additionally, sol-gel coatings can bestow further desirable properties, such as prevention of ice accumulation, oxidation resistance and abrasion resistance [13]–[15]. During the past decade, the development of hybrid organic-inorganic sol-gel coating technology has overcome the concerns around defects such as cracking, peel off and decohesion, which affected early so l- gel coating formulations. Nevertheless, long-term exposure to moisture can negatively influence the adhesion and cohesion properties of many coating systems [10], [16].

Coating cracking and delamination from the Substrate can occur due to changes in chemical and mechanical properties of the coating and the interfacial layer between the coating and the Substrate. Typically, during the ionic diffusion processes, an oxide layer is created on the metal substrate. This new interfacial layer reduces the adhesion of the coating to the Substrate and can induce stresses in the coating. Compressive stresses can have a positive impact on mechanical properties by sealing surface cracks, although high compressive stresses can lead to buckling of the coating film. Conversely, cracks and delamination of the coating are observed when tensile stresses

exceed the elastic limit in the thin layer [17], [18].

In this work, the performance of a fluorinated sol-gel coating with a 1H,1H,2H,2H- Perfluorodecyl triethoxy silane and based hybrid organic-inorganic sol-gel coatings were systematically investigated in controlled conditions. A solution of 3.5% w/v sodium chloride was utilized to simulate the extended exposure relevant to applications.

II. Experimental Work

All preparations, testing and characterizations were performed at material and engineering research institute (MERI) labs at Sheffield Hallam University.

A. Materials

All materials and chemicals used in this work were of analytical grade. Experiments were performed in an oxygenated environment and at ambient temperature (20o C +/- 2o C). All glassware was cleaned with an industrial aqueous cleaner then rinsed with acetone and finally deionized water.

1) Substrate Preparation

Commercially available Q-panels made of aluminium alloy AA2024 T3 with dimensions (102 mm × 25 mm × 1.6 mm) were supplied by Q-Lab for use as test substrates. The chemical composition of the Substrate is given in Table I [19].The as-received panels were washed with a proprietary surfactant-based cleaner and rinsed with deionized water, then washed with acetone to remove organic residues such as oil, grease and fats present on the surface. These panels were then placed in an ultrasonic water bath for five minutes for additional cleaning with CEE BEE® Super Bee 999 alkaline cleaner, followed by rinsing with deionized water and drying with pressurized nitrogen gas. The panels were then kept in a desiccator until the coating was applied.

Table I. Composition of Aluminum Alloy AA2024 T3 [19]

Element	Si	Fe	Cu	Mn	Mg	Cr	Zn	It	Other Elements
Wt(%)	0.50	0.50	0.38-4.9	0.30-0.9	1.2-1.8	0.10	0.25	0.15	0.05-0.15

2) Sol-Gel Preparation

The hybrid organic-inorganic sol-gel used in this study was synthesized from tetraethyl orthosilicate silane (TEOS), and trimethoxymethylsilane (MTMS) purchased from Sigma-Aldrich. These precursors were mixed in isopropanol by dropwise additions of deionized water (DI) at the molar ratio of 18: 14: 17: 220 respectively. The sol-gel was then enhanced with polysiloxane (PSES) solution, which was obtained by adding 12 mol% of (– O.H.) terminated polysiloxane polymer into the hybrid sol-gel [20]. This formulation, which was used as the unmodified baseline coating, was labelled SBX. The modified, fluorinated hybrid sol-gel, labelled as F-SBX, was prepared by adding 1.5 vol.% of 1H,1H,2H,2H-perfluorodecyltriethoxysilane (PFDTES) from Sigma-Aldrich into the original SBX sol-gel formulation. Dropwise additions of nitric acid 65-70% ACS Reagent grade (HNO3) from Sigma Aldrich were made as a catalyst for the hydrolyzing and condensation reactions; the formulation was then stirred for 24 hours.

3) Film Deposition

The coating was applied to the pre-cleaned aluminium alloy substrates by spray coating. The distance from the gun to the Substrate was maintained at approximately 150 mm, and the coating was built up over three passes. After deposition, the coatings were left in ambient air for 10 min before being thermally treated at 80° C for 4 hours. Table II shows sample codes used to identify samples.

Table II. Sample identification table

Identifier	Base Composite Sol-gel	(PFDTES) V/V%	Curing Temperayure
SBX-80	TEOS+MTMS+PSX	-	80° C
F-SBX-80	TEOS+MTMS+PSX	1.5%	80° C
Bare AA2024 T3	-	-	-

B. Coating Testing and Characterization

The thickness of the coated samples was measured using an Elcometer 456 Model Coating Thickness Gauge and confirmed with the scanning electron microscope (SEM) cross-section imaging. The Elcometer 1540 Adhesion Tester was also used to determine the coating adhesion in accordance with ASTM D3359 [21].

An FEI-QUANTA 650 scanning electron microscope (SEM), with an X-MAX 80 mm2 energy-dispersive X-ray (EDX) spectrometer (Oxford Instruments), was used to analyze the morphology and chemical composition of coated samples.

The hydrophobicity of the sol-gel coatings was determined by performing water contact angle measurements using a Dataphysics OCA 15EC Goniometer, with deionized water (DI) used as the solvent. A minimum of three analyses was performed across the surface of each sample, and the mean water contact angle value calculated by the Dataphysics OCA software [22].

Information regarding the composition and rehydration behaviour of the sol-gel coatings was obtained using a Thermo Nicolet Nexus FTIR spectrophotometer with a Quest-single reflection attenuated total reflectance sampling accessory, a diamond ATR crystal and a liquid nitrogen-cooled Mercury Cadmium Telluride (MCT) detector Tests were conducted by placing a dried film of sol-gel directly onto the ATR crystal and spectra were acquired using a resolution of 4 cm−1 and 64 scans.

Electro chemical tests were performed on the coatings to assess their corrosion resistance. Tests were conducted using a Princeton Applied Research PARSTAT 2273 and three-electrode cell, with the coated Substrate as the working electrode, a saturated calomel electrode (SCE) reference electrode and platinum as the counter electrode. The corrosion behaviour of the uncoated and sol-gel coated aluminium alloy was evaluated using potentiodynamic polarization scans and electrochemical impedance spectroscopy (EIS). The EIS test specimens were prepared by masking the samples with a beeswax-colophony resin mixture, leaving an exposed area of 1.00 mm2 in the centre of the sample. All electrochemical tests were carried out at room temperature (20o C +/- 2o C) and in aerated 3.5 % w/v NaCl solution. Prior to polarisation, the

electrode potential was monitored for approximately 1 hour in the NaCl solution until it reaches stability. The sample was polarised at a scan rate of 1.667 mVs-1 from the initial potential of -250 mV vs OCP to +750 mV vs SCE. The EIS measurements were recorded between 100 kHz to 10 MHz with a sinusoidal AC RMS value of 10 mV [23], [24].

III. Results and Discussion

A. Coating Thickness and adhesion Measurement

The thickness of the coatings was determined using an Elcometer Coating Thickness Gauge and measured as 18 ± 2 µm and confirmed by scanning electron microscope cross-section imaging as shown in Fig.1, the coating adhesion cross-hatching test showed that the SBX coating fall in the 5B category and F-SBX fall in the 5B-4B category which is determined that both systems are in very good adhesion on A.A. 2024-t3 as shown in Fig. 2.

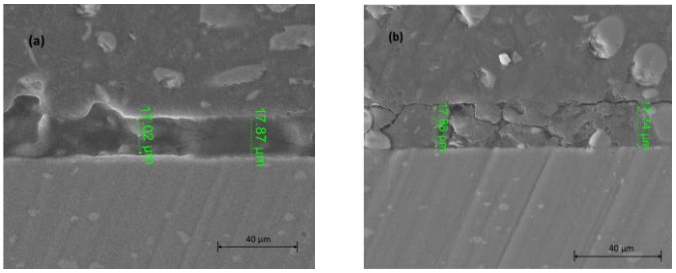

Figure 1. SEM images of cross-section of (a) SBX sol-gel coated, (b) fluorinated F-SBX sol-gel samples

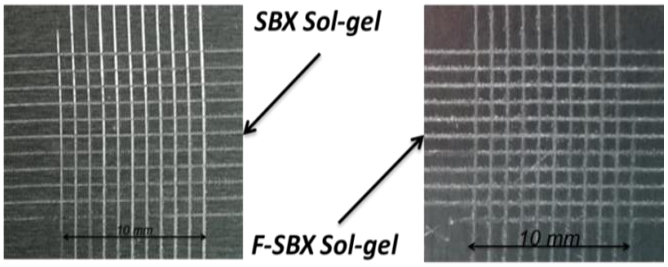

Figure 2. The cross-cut adhesion test of different sol-gel coating systems

1) Confirmation of PFDTES Addition In F-SBX Formula

Successful incorporation of the fluorinated precursor into the sol-gel was confirmed by comparing the infrared spectrum obtained from the F-SBX80 coating to the unmodified SBX-80, as shown in Fig.3. The presence of the C-F bonds can be confirmed by examining the I.R. spectral range between 1400-900 cm-1 Evidence of the C-F, and C-F2 bonds can be observed in spectrum, by the presence of bands at 1140 and 1250 cm−1 is provided by the presence of the bands highlighted in the spectrum correspondingly [25].

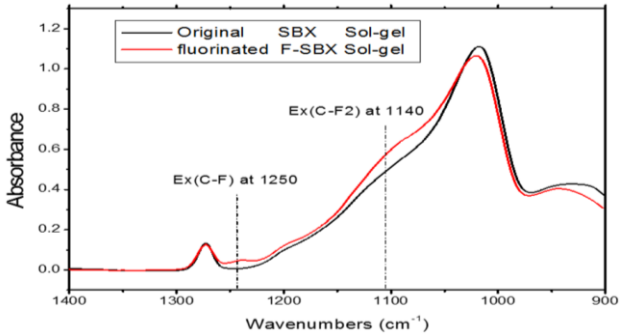

Figure 3. ATR-FTIR spectra showing the effect of PFDTES addition to the unmodified SBX-80 sol-gel

2) Water Contact Angle of SBX and F-SBX Coatings

Fig. 4, showed a typical bar chart mean values of the water contact angle measurement droplets on both coating systems. In Figure 5 (a) the results of measured average water contact angle (WCA) of the original SBX-80 coating were 67° ± 2°, and as shown in 4(b), the result of WCA on modified F-SBX-80 Sol-gel coating was 118° ± 2°.

The higher water contact angle recorded for the F-SBX-80 shows that its wettability is lower than that of the SBX-80 as a result of increase hydrophobicity of the fluorinated F-SBX-80 coating [26].

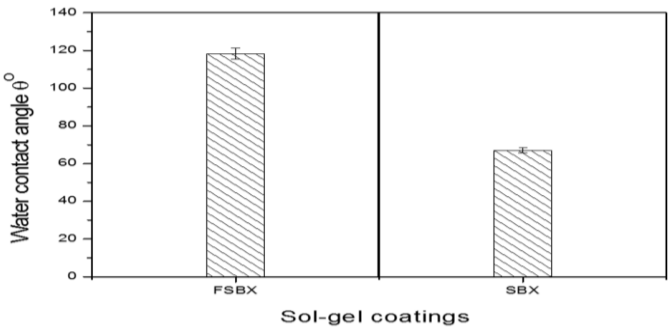

Figure 4, Bar chart showing mean values of WCA of F- SBX-80 and SBX-80 coatings

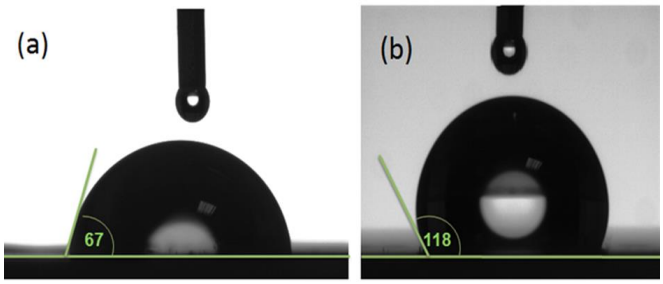

Figure 5. Optical images showing water droplets with annotations indicate contact angle on (a) SBX-80 and (b) fluorinated F-SBX-80 coatings surface.

3) The Effect of Prolonged Water Exposure on Sol-gel Coating Films

ATR-FTIR spectroscopy was used for comparing the response of SBX-80 and F-SBX-80 coating films exposed in an aqueous environment for five days to assess the relative water

uptake of both coatings. The evaluation was made by examining the differences in the O.H. stretching region between 3000 and 3400 cm-1. Fig.6 (a) shows a noticeable change in the O.H. stretch after immersion for the unmodified SBX-80 coating, which can be attributed to water uptake. By comparison, Fig.6 (b) shows that no significant changes were observed in this region in the case of the fluorinated F-SBX-80 coating. This suggests that there is minimal water uptake by the fluorinated coating.

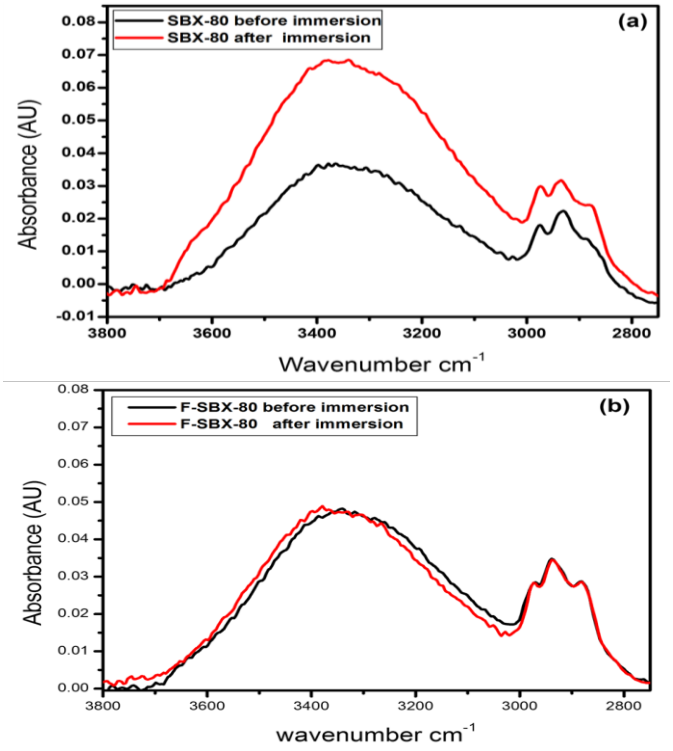

Figure 6, FTIR spectra showing the change in the O.H. stretch region before and after water immersion for (a) SBX-80 and (b) F-SBX-80 films

B. *Electrochemical Corrosion Testing Analysis*

1) *Potentiodynamic polarisation*

Potentiodynamic polarization scans were performed on all samples with hybrid sol-gel coatings. The results for SBX-80 and F-SBX-80 are presented in Fig.7, along with the result of a test conducted on bare 2024-T3 aluminium alloy for comparison. The values of corrosion potential (Ecorr) and measured current density (Icorr) were obtained by extrapolation of cathodic and anodic curves by using Tafel extrapolation method and results are shown in Table III. The results show that the coatings reduced the measured current when compared to the uncoated aluminium alloy and shifted the corrosion potential to more noble values. This phenomenon was more apparent in the F-SBX-80 coating, which showed a shift of 199 mV compared to the uncoated 2024-T3. The initial observation that corrosion protection offered by both sol-gel coatings is due to excellent barrier properties. Nonetheless, the shift in Ecorr indicates that the anode is inhibited to a greater degree than the cathode; this is attributes to the fluorine-carbon atoms bridging to the Substrate [24], [27].

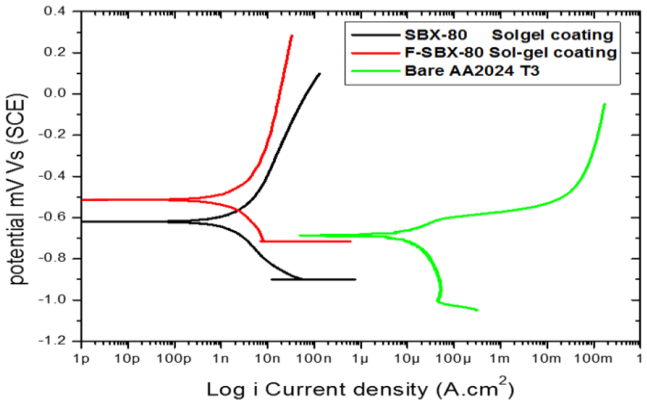

Figure 7. PDS Polarization curves for the bare AA 2024-T3 alloy and sol-gel coatings on AA 2024-T3 after 1 hr of immersion in 3.5% NaCl solution.

Table III. Parameters obtained from table extrapolation for bare AA 2024 T3, sol-gel coatings immersed in 3.5 % w/v NaCl solution

Sample	E_{corr} [m V vs SCE]	I_{corr}[A/cm^2]	OCP[m V vs SCE]
Bare-AA 2024	-662±2	7.10×10^{-6}	-640
SBX-80 coating	-608±2	1.02×10^{-9}	-708
F-SBX-80 coating	521±2	1.22×10^{-9}	-658

2) *Electrochemical Impedance Spectroscopy (EIS) Analysis*

Tests were performed over a period of 14 days. Fig. 8 (a) and (b) show impedance magnitude and phase angle plots for F-SBX-80, while 8 (c) and (d) show the same plots for the SBX-80 coating.

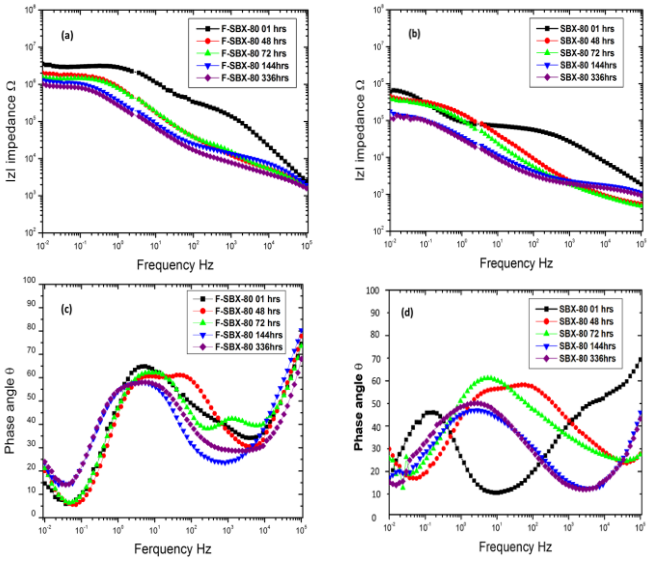

Figure 8.Impedance magnitude and phase angle plots for F-SBX-80 and SBX-80 coated samples

The overall impedance was increased by approximately one order of magnitude for the F-SBX-80 coated samples compared to the SBX-80 samples, with impedance values of 6.8x106 Ω and 6.8x105 Ω respectively, after one hour. At frequencies between 100 to 105 Hz, the impedance curve for the F-SBX-80 sample reveals pure capacitive behaviour (C), and then the

impedance slowly increased from at about 6.6x105 Ω in the middle range of the frequencies and finally reached the point where the rate of increase impedance is small at the low frequencies. Likewise, in the EIS measurements of the SBX-80 coated sample, a noticeable drop in impedance was observed at about 1.0x105 Ω after 14 days. On the other hand, this SBX coating still revealed higher impedance compared to the bare Substrate.

The phase angle plots acquired on the first day for both coating systems show that the F-SBX-80 and SBX-80 coated sample exhibit two semi-circles, then after 48 hrs of immersion, the phase angle plot for the SBX-80 coated samples indicated the presence of three-time constants. However, the F-SBX-80 coated samples kept two time-constants to the 14th day of the test, The increased Rct values obtained from F-SBX are consistent with anodic inhibition obtained through a fluorine-influenced interface[27].

3) Electrochemical Equivalent Circuits Fitting for Both Sol-gel Coatings

Fig.9, shows Nyquist plots for both SBX and F-SBX coatings in 01 to 336 hrs. These plots were used to obtain and fitting the data to some models of equivalent circuits by using ZSimpwin electrochemical impedance spectroscopy (EIS) data analysis software.

The tables IV and V below demonstrate the fitted data obtained from EIS spectra for the SBX-80 and the F-SBX-80 sol-gel coating after various immersion times in 3.5% w/v NaCl solution. The equivalent circuits were used to simulate the corrosion mechanism on the coated sample in 01 hr, 48hrs and 144 hrs. In these circuits, a time-constant element (Q), was used instead of an ideal capacitor C, to account for current leakage in the capacitor and/or frequency dispersion effect of the alternating current signals [23], [24].

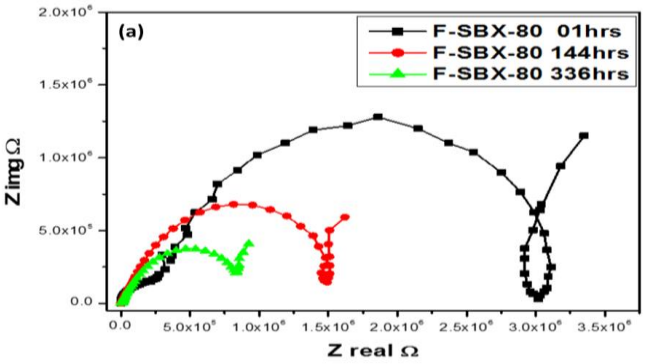

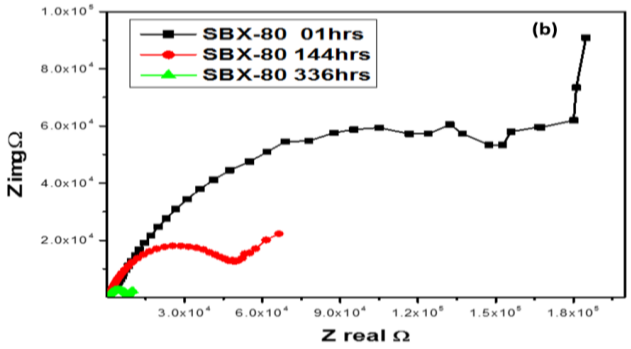

Figure 9, Nyquist plots for (a) F-SBX and (b) SBX coatings

Table IV. The fitted data, obtained from EIS spectra for the SBX sol-gel coating after various immersion times

		immersion time (h)		
Sample	Element	01	48	144
	Circuit	R(Q(R(QR)))	R(Q(RO)(QR))	R(Q(RO)(RQ))
	R_s	10	18	45
	Q_{ct}	8.913E-10	9.326E-10	1.915E-9
	n	1	1	0.900
	R_{ct}	2.220E6	6.522E04	3.776E4
	O_{ct}	-	2.823E-7	4.866E-7
	B	-	0.469	0.618
	Q_{iL}	3.800E-8	1.103E-7	3.592E-7
	n	0.772	0.803	0.800
	R_{iL}	3.319E6	9.675E5	2.136E4

Table V. The fitted data obtained from EIS spectra for the F-SBX sol-gel coating after various immersion times

		immersion time (h)		
Sample	Element	01	48	144
	Circuit	R(Q(R(QR)))	R(Q(R(Q(RW))))	R(Q(R(Q(RW))))
	R_s	100	205	195
	Q_{ct}	1.085E-7	2.059E-7	6.1181E-6
	n	0.649	0.800	0.752
	R_{ct}	7.294E4	817	110
	Q_{iL}	4.934E-6	1.236E-6	9.815E-6
	n	0.827	0.800	0.818
	R_{iL}	7.790E5	3.504E6	1.475E5
	W_{iL}	-	2.317E-5	8.084E-5

The elements used for the equivalent circuits were: solution resistance (R_s), coating resistance (R_{ct}), coating constant phase elements (Q_{ct}), intermediate oxide layer resistance (R_{iL}), intermediate oxide layer capacitance (Q_{iL}), fininte Warburg-circuit element (O) and Warburg-circuit element (W) [28]. At, the first hour of immersion, both samples illustrate the same behaviour with three resistance and two time-constants respectively, as shown in Fig. 10 (a) and (c). However, after 48 hours of immersion of both coated samples SBX and F-SBX started behaving individually. SBX-80 coating results indicate that there are three-time constants.

The first one arises in the high-frequency range and may be attributed to capacitive effects at the coating/aluminium/ aluminium oxide interfacial layer in the coating, the second one is due to diffusion properties of the coating, and the third one may be attributed to Warburg-circuit element (W) as result of diffusion to the substrate surface as shown in Fig. 10 (d). On the other hand, the F-SBX-80 coated sample kept two time-

constants with a fininte Warburg-circuit element (O) as shown in Fig. 10 (b). This (O) element is thought to originate from the hydrophobic nature of the fluorinated group (- CH_2 CH_2 (CF2) $_7CF_3$) from the PFDTES additive, which prevents the diffusion of electrolyte into the fluorinated coating.

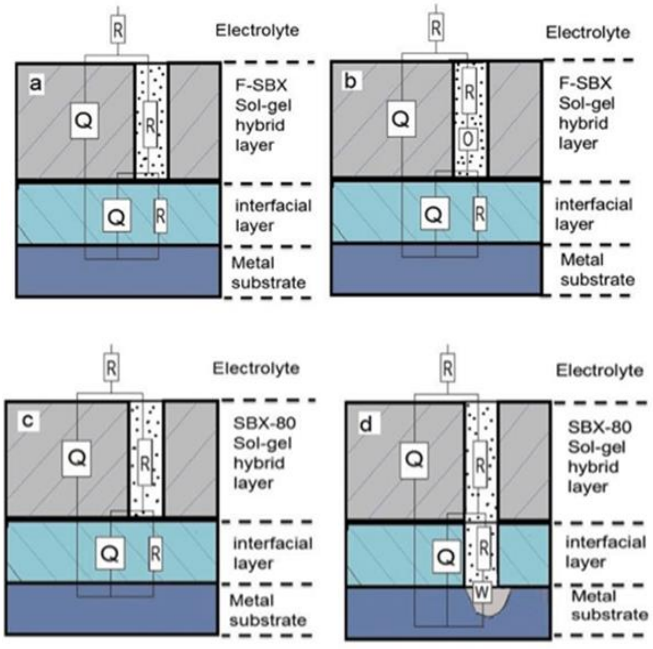

Figure 10. The modelling of (a, b) F-SBX-80 and (c, d) SBX-80 coating systems

As can be seen, the behaviour of SBX-80 coating initially subjugated by two semi-circles, which represent the resistance of the coating and interfacial layers. As immersion time increases, the resistive nature of the coating reflected the onset of degradation.

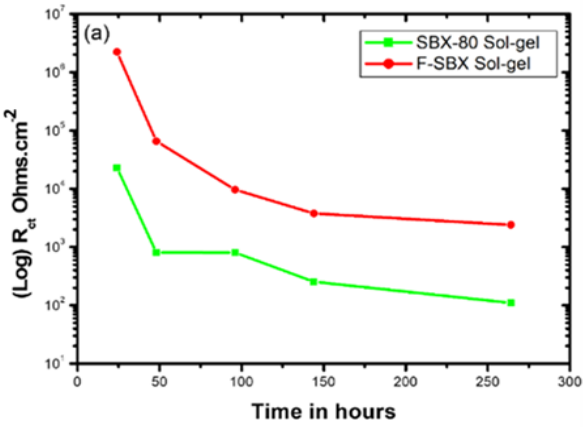

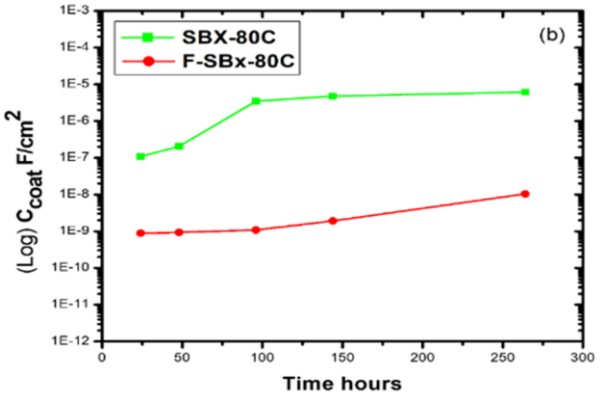

Figure 11. Graphs showing (a) Coating Pore Resistance and (b) Coating constant phase elements for SBX-80 and F-SBX-80 Coatings

The deterioration of the corrosion protective characteristic of the coatings was studied between 24 and 336 hours in immersion, as shown in figure 11. A value of R_{ct} of F-SBX at the first hour of immersion started from an initial amount of 2.22×10^6 ohms.cm^{-2} then after 48 hrs was dropped to 6.8×10^4 ohms.cm^{-2}, then it was relatively dropped after 96 hrs to reach about 4.0×10^3 ohms.cm^{-2} at the end of the test. These resistances have a corresponding coating constant phase element (Q_{ct}) with capacitance behaviour of 1.08×10^{-7} and 8.91×10^{-10} F.cm^{-2} for SBX-80 and F-SBX-80 respectively after one hour of immersion. Due to the degradation of coating, the SBX-80 coating capacitance increases after 144 hrs of immersion to 4.7×10^{-6} F.cm^{-2} [29]. On the other hand, the F-SBX-80 showed levelling off in the same magnitude about 2.6×10^{-9} F.cm^{-2}.

The coating resistance (R_{ct}) of the SBX-80 coating in the First hour of immersion, was about 7.3×10^4 ohms.cm^{-2} is approximately one order of magnitude less than the F-SBX-80 sol-gel coating; it indicates that the SBX-80 coating samples still have a satisfactory coating resistance. However, after 48 hours, the coating resistance of the SBX-80 coating decreased markedly to 8.0×10^2 ohms.cm^{-2}, before continuing to decline throughout the remainder of the test to reach 1.1×10^2 ohms.cm^{-2}. As exposure time increase, the reduction is due to the microcracking and diffusion of the SBX sol-gel coating.

4) Crack Growth After Long Immersion

Both coated samples SBX-80 and F-SBX-80 demonstrated an ability to provide corrosion protection to the aluminium alloy substrate during immersion. Furthermore, visual examination of samples immediately after immersion showed no apparent degradation or damage to the coating. However, after longer immersion times (greater than five days), the SBX-80 coating was susceptible to the formation of microcracks when dried in ambient atmospheric conditions.

The cracks were observed to be around 1-3 µm wide on the surface, as shown in the SEM images in Fig. 12(a) and (b). Exposure of the aluminium alloy substrate as a result of coating cracking has the potential to detrimentally affect the subsequent corrosion protection, having implications for situations where wet/dry cycling is experienced. By comparison, the F-SBX-80 coating showed excellent resistance to cracking under similar

circumstances, as shown in Fig. 12(c) and (d). The contact angle measurements showed that the F-SBX-80 was more hydrophobic than the SBX-80, while the FTIR confirmed that the unmodified sol-gel had a higher propensity for water uptake. The presence of water in the film could lead to swelling and loss of coating-substrate adhesion, leading to the cracking observed in the case of the SBX-80.

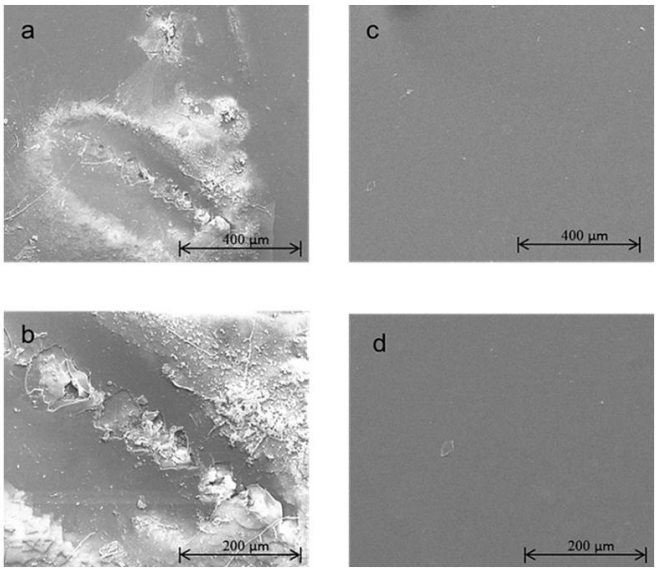

Figure 12.Secondary electron SEM micrographs of the long immersion effect on both coatings (a), (b) SBX-80 and (c), (d) F-SBX-80

IV. Conclusion

The addition of a 1H, 1H, 2H, 2H-Perfluorodecyltriethoxy silane (PFDTES) precursor has the potential to enhance the corrosion performance of the basic TEOS and MTMS Hybrid organic-inorganic sol-gel coating on AA2024-T3 substrates and this confirmed by the electrochemical corrosion testing techniques by enhancing the hydrophobicity of coating when it is compared to other coatings with the same curing temperature of 80oC. Furthermore, the fluorinated group from PFDTES in the hybrid organic-inorganic sol-gel coating exhibits improved post-exposure cracking resistance after prolonged immersion compared to the unmodified sol-gel coating; this is attributable to the flexibility properties of the new coating. Moreover, exploiting the hydrophobic nature of the PFDTES precursor in low concentrations is potentially beneficial for applications that require self-cleaning and anti-fouling properties.

V. Acknowledgement

The authors would like to acknowledge the facility support by Sheffield Hallam University technical staff and to the Libyan Scholarship Program for the financial fund.

References

[1] W. Trabelsi, L. Dhouibi, F. Matoussi, and E. Triki, "Modification of corrosion behavior of stainless steels with a poly-m-methoxytoluene coating," Synth. Met., vol. 151, no. 1, pp. 19–24, May 2005, [Online]. Available: https://linkinghub.elsevier.com/retrieve/pii/S0379677905000974.

[2] S. Ammar, K. Ramesh, B. Vengadaesvaran, S. Ramesh, and A. K. Arof, "A novel coating material that uses nano-sized SiO2particles to intensify hydrophobicity and corrosion protection properties," Electrochim. Acta, vol. 220, pp. 417–426, 2016.

[3] T. Zheng, Y. Hu, Y. Zhang, and F. Pan, "Formation of a hydrophobic and corrosion resistant coating on magnesium alloy via a one-step hydrothermal method," J. Colloid Interface Sci., vol. 505, pp. 87–95, 2017.

[4] B. Yin et al., "Novel strategy in increasing stability and corrosion resistance for super-hydrophobic coating on aluminum alloy surfaces," Appl. Surf. Sci., vol. 258, no. 1, pp. 580–585, 2011.

[5] E. Almeida, T. C. Diamantino, and O. de Sousa, "Marine paints: The particular case of anti-fouling paints," Prog. Org. Coatings, vol. 59, no. 1, pp. 2–20, 2007.

[6] X. jun Cui, X. zhou Lin, C. hai Liu, R. song Yang, X. wen Zheng, and M. Gong, "Fabrication and corrosion resistance of a hydrophobic micro-arc oxidation coating on AZ31 Mg alloy," Corros. Sci., vol. 90, pp. 402–412, 2015, [Online]. Available: http://dx.doi.org/10.1016/j.corsci.2014.10.041.

[7] D. L. Marks, C. Vinegoni, J. S. Bredfeldt, and S. A. Boppart, "Interferometric differentiation between resonant Coherent Anti-Stokes Raman Scattering and nonresonant four-wave-mixing processes," no. 1, Art. no. US 2016/0185978 A1, Feb. 2004, [Online]. Available: http://arxiv.org/abs/physics/0403007.

[8] M. R. Detty, R. Ciriminna, F. V. Bright, and M. Pagliaro, "Environmentally benign sol-gel anti-fouling and foul-releasing coatings.," Acc. Chem. Res., vol. 47, no. 2, pp. 678–687, 2014.

[9] R. Akid, H. Wang, M. Gobara, T. J. Smith, and J. Gittens, "Green coatings for industrial applications," Corros. Manag., no. 100, pp. 11–14, 2011.

[10] H. Wang, R. Akid, and M. Gobara, "Scratch-resistant anti-corrosion sol–gel coating for the protection of AZ31 magnesium alloy via a low temperature sol– gel route," Corros. Sci., vol. 52, no. 8, pp. 2565–2570, 2010.

[11] S. Chen, L. Li, C. Zhao, and J. Zheng, "Surface hydration: Principles and applications toward low-fouling/nonfouling biomaterials," Polymer (Guildf)., vol. 51, no. 23, pp. 5283–5293, Oct. 2010, [Online]. Available: https://linkinghub.elsevier.com/retrieve/pii/S0032386110006968.

[12] U. Eduok et al., "Anticorrosion/anti-fouling properties of bacterial spore-loaded sol-gel type coating for mild steel in saline marine condition: a case of thermophilic strain of Bacillus licheniformis," RSC Adv., vol. 5, no. 114, pp. 93818–93830, 2015, [Online]. Available: http://dx.doi.org/10.1039/C5RA16494J.

[13] O. Lev et al., "Sol−Gel Materials in Electrochemistry," Chem. Mater., vol. 9, no. 11, pp. 2354–2375, Nov. 1997, [Online]. Available: http://pubs.acs.org/doi/abs/10.1021/cm970367b%255Cnhttp://dx.doi.org/10.1021/cm970367b%255Cnhttp://pubs.acs.org/doi/full/10.1021/cm970367b%255Cnhttp://pubs.acs.org/doi/pdf/10.1021/cm970367b%255Cnhttp://pubs.acs.org/doi/abs/10.1021/cm970367b.

[14] D. Wang and G. P. Bierwagen, "Sol–gel coatings on metals for corrosion protection," Prog. Org. Coatings, vol. 64, no. 4, pp. 327–338, Mar. 2009, [Online]. Available: https://linkinghub.elsevier.com/retrieve/pii/S0300944008002038.

[15] S. S. Pathak and S. Khanna, "Sol–gel nano coatings for corrosion protection," Met. Surf. Eng., vol. 12, no. 1, pp. 304–329, 2012.

[16] S. Zhang, Z. Xianting, W. Yongsheng, C. Kui, and W. Wenjian, "Adhesion strength of sol-gel derived fluoridated hydroxyapatite coatings," Surf. Coatings Technol., vol. 200, no. 22-23 SPEC. ISS., pp. 6350–6354, 2006.

[17] C. W. Paul, "Hot melt adhesives," in Adhesion Science and Engineering, 1st ed., A.M, Ed. Amsterdam, The Netherlands: ELSEVIER SCIENCE B.V., 2002, pp. 711–757.

[18] J. A. Lewis, "Non-silicone biocide-free anti-fouling solutions," in Advances in Marine Antifouling Coatings and Technologies, vol. 123, no. 1995, Woodhead Publishing Limited, 2009, pp. 709–724.

[19] ASTM International, "ASTM code B209 − 14 Standard Specification for Aluminum and Aluminum-Alloy Sheet and Plate," vol. 25. ASTM International, West Conshohocken, p. 16, 2016.

[20] H. Wang and V. Kumar, "Transparent and conductive polysiloxanes / PEDOT:PSS nanocomposite thin films with a 'water-impermeable' property to significantly enhance stability of organic–inorganic hybrid

solar cells," RSC Adv., vol. 5, no. 13, pp. 9650–9657, 2015, [Online]. Available: http://xlink.rsc.org/?DOI=C4RA14079F.

[21] C. Coatings, R. C. Products, E. Applica-, S. Tape, T. Paint, and R. Materials, "Standard Test Methods for Measuring Adhesion by Tape Test," ASTM Int., no. December 2007, pp. 1–8, 2012.

[22] G. Bracco and B. Holst, "Contact Angle andWetting Properties," in Springer Series in Surface Sciences, vol. 51, no. 1, Springer, 2013.

[23] Gamry instruments, "Basics of Electrochemical Impedance Spectroscopy," Application Note, 2016. http://scholar.google.com/scholar?hl=en&btnG=Search&q=intitle:Basics+of+Electrochemical+Impedance+Spectroscopy#2 (accessed Feb. 01, 2017).

[28] W. S. Tait, Electrochemical impedance spectroscopy fundamentals, an introduction to electrochemical corrosion testing for practicing engineers and scientists. Racine, Wisconsin, USA: PairODocs Publications, 1994.

[29] J. Brassard, D. K. Sarkar, and J. Perron, "Fluorine Based Superhydrophobic Coatings," Appl. Sci., vol. 2, no. 2, pp. 453–464, 2012.

[30] D. Kumar et al., "Development of durable self-cleaning coatings using organic-inorganic hybrid sol-gel method," Appl. Surf. Sci., vol. 344, pp. 205–212, 2015, doi: 10.1016/j.apsusc.2015.03.105.

[31] T. Kobayashi and H. M. Hugel, "Special issue, organo-fluorine chemical science-inventing the fluorine future," in Applied Sciences, B